ELSEVIER

Ceramics International 30 (2004) 751–755

CERAMICS INTERNATIONAL

www.elsevier.com/locate/ceramint

Dielectric properties of multiple-octahedral ceramic system $Pb[(\langle Mg,Zn\rangle_{1/3}Nb_{2/3})_{0.8}Ti_{0.2}]O_3$ with Ta substitutions for Nb

Jee-Su Kim, Nam-Kyoung Kim*

Department of Inorganic Materials Engineering, Kyungpook National University, Daegu 702-701, South Korea

Received 25 February 2003; received in revised form 18 August 2003; accepted 12 September 2003

Available online 17 March 2004

Abstract

A fixed fraction (20 mol%) of $PbTiO_3$ was introduced into $Pb[(Mg,Zn)_{1/3}Nb_{2/3}]O_3$ with systematic substitutions of Nb by Ta. Powders were prepared by two-stage reactions with repeated calcination to improve perovskite formation. Developed structures in the calcined powders were determined by X-ray diffraction. The low-frequency dielectric constant and loss values of the ceramics were measured. Dielectric constant spectra were further analyzed to investigate the diffuseness modes. Internal microstructures were examined using a scanning electron microscope.

Keywords: A. Powders: solid-state reaction; A. Precursors; B. X-ray methods; C. Dielectric properties; D. Perovskites

1. Introduction

In $Pb(B',B'')O_3$-type complex-perovskite relaxor ferroelectric compositions (and solid solutions thereof), magnitudes of the dielectric constant maxima decreased, whereas those of the dielectric loss as well as corresponding temperatures of the maxima increased with increasing measurement frequency. $Pb(Mg_{1/3}Nb_{2/3})O_3$ and $Pb(Zn_{1/3}Nb_{2/3})O_3$ (PMN and PZN, hereafter) are two typical examples which exhibit such characteristics. In contrast, $PbTiO_3$ (PT) is a so-called normal ferroelectric, possessing rather sharp dielectric constant maxima and little dielectric dispersion of frequency dependence.

Many investigations of the PMN-PZN-PT system [1–6] have been reported thus far. The pseudoternary compositions have also been the base materials for many applications to dielectric and electrostrictive areas. It has been reported that a very high maximum dielectric constant of 37,900 (1 kHz) at 85 °C was obtained in the PMN-PZN system with the introduction of 20 mol% PT (i.e., $(0.8-z)$PMN-zPZN-0.2PT), when $z = 0.2$ and 1/4 of Nb was replaced by Ta [7]. Therefore, the value of z was further increased to 0.4 (System I) and 0.6 (System II) in the present study with additional substitutions of Nb by Ta, and the resulting dielectric properties were investigated. It was hoped that even higher values of the maximum dielectric constant could be attained for potential applications to high volumetric-efficiency chip capacitors. In order to increase perovskite formation yields, powders were prepared by solid-state reactions using a B-site precursor method [8], which is basically identical to (but more comprehensive than) the columbite process [9,10].

2. Experimental

Compositions of the 20 mol% $PbTiO_3$-introduced $Pb[(Mg,Zn)_{1/3}Nb_{2/3}]O_3$ system with additional Ta substitutions for Nb can be expressed as $Pb[(Mg_{0.4}Zn_{0.4})_{1/3}(Ta_{0.8-x}Nb_x)_{2/3}Ti_{0.2}]O_3$ (System I) and $Pb[(Mg_{0.2}Zn_{0.6})_{1/3}(Ta_{0.8-y}Nb_y)_{2/3}Ti_{0.2}]O_3$ (System II). Several compositions of the two systems (x, y = 0.0–0.8 at regular intervals of 0.2) were selected for investigation. Starting materials were high-purity oxide chemicals of PbO (99.5%), MgO (99.9%), ZnO (99.8%), Ta_2O_5 (99.9%), Nb_2O_5 (99.9%), and TiO_2 (99.9%). The moisture contents of the raw materials and of the separately-synthesized B-site precursor powders were measured and introduced into the batch calculations to

* Corresponding author. Tel.: +82-53-950-5636; fax: +82-53-950-5645.
E-mail address: nkkim@knu.ac.kr (N.-K. Kim).

0272-8842/$30.00
doi:10.1016/j.ceramint.2003.09.011

keep the compositions as closely to the nominal values as possible.

B-site precursor powders of $[(Mg_{0.4}Zn_{0.4})_{1/3}(Ta_{0.8-x}Nb_x)_{2/3}Ti_{0.2}]O_2$ and $[(Mg_{0.2}Zn_{0.6})_{1/3}(Ta_{0.8-y}Nb_y)_{2/3}Ti_{0.2}]O_2$ formulae were prepared by solid-state reactions for 2 h at 1050–1200 °C (depending on composition). The calcined lumps were milled, dried, and reacted again at identical conditions to promote phase formation. After the addition of PbO to the precursor powders in appropriate proportions, the mixtures were calcined at 850 and 900–1000 °C for 2 h each, with intermediate milling and drying steps. Developed structures after each heat treatment stage were determined by powder X-ray diffraction (XRD). The prepared powders (with the addition of 2 wt.% polyvinyl alcohol aqueous solution) were isostatically pressed into pellet-type samples. The preforms were then fired for 1 h (dwell time) at 1050–1200 °C in a multiple-enclosure inverted-crucible setup [11]. Sintered pellets were ground/polished and Au-sputtered for electrical contacts. Dielectric constant and loss values of the ceramics were measured on cooling at 1 kHz–1 MHz. Microstructures of the fractured samples were examined using a scanning electron microscope (SEM).

3. Results and discussion

XRD results of the B-site precursor $[(Mg_{0.4}Zn_{0.4})_{1/3}(Ta_{0.8-x}Nb_x)_{2/3}Ti_{0.2}]O_2$ powders are displayed in Fig. 1a. Only a trirutile structure ($MgTa_2O_6$, ICDD No. 32-631) was identified at $x = 0.0$ of $[(Mg_{1/3}Ta_{2/3})_{0.4}(Zn_{1/3}Ta_{2/3})_{0.4}Ti_{0.2}]O_2$, indicating that the equimolar component of $ZnTa_2O_6$ (tri-αPbO_2 structure, ICDD No. 39-1484) had completely dissolved in the trirutile solid solution, in spite of quite different crystal structures. The TiO_2 component (20 mol%) of a rutile structure (ICDD No. 21-1276) had also been dissolved into the trirutile. In contrast, tri-αPbO_2 and rutile structures (the former one with higher intensities) coexisted at $x = 0.2$ and 0.4. At $x = 0.6$, the X-ray pattern was quite similar to that of $x = 0.4$, except for the emergence of a columbite structure. The columbite then became dominant over the rutile and tri-αPbO_2 at $x = 0.8$, $[(Mg_{1/3}Nb_{2/3})_{0.4}(Zn_{1/3}Nb_{2/3})_{0.4}Ti_{0.2}]O_2$.

X-ray patterns of the $[(Mg_{0.2}Zn_{0.6})_{1/3}(Ta_{0.8-y}Nb_y)_{2/3}Ti_{0.2}]O_2$ system are shown in Fig. 1b. At $y = 0.0$, i.e., $[(Mg_{1/3}Ta_{2/3})_{0.2}(Zn_{1/3}Ta_{2/3})_{0.6}Ti_{0.2}]O_2$, trirutile and tri-$\alpha PbO_2$ structures were observed, which indicates that the 20 mol% component of rutile had dissolved completely in the trirutile, when the comparative similarity between the reported patterns of the two (ICDD Nos. 21-1276 and 32-631) is considered. Moreover, part of the $ZnTa_2O_6$ component had also somehow been assimilated to the trirutile structure, thus resulting in somewhat higher intensities of the trirutile. Meanwhile, tri-αPbO_2 and rutile structures coexisted at $y = 0.2$ and 0.4 (similar to the patterns of $x = 0.2$ and 0.4), but the intensities of the rutile were substantially

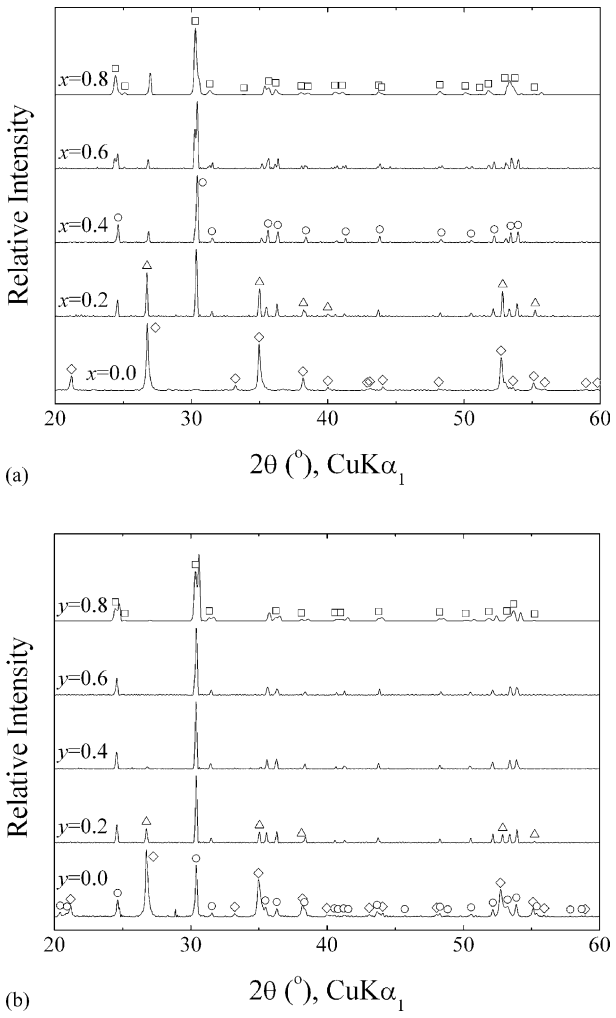

Fig. 1. Powder X-ray diffractograms of the B-site precursor systems (a) $[(Mg_{0.4}Zn_{0.4})_{1/3}(Ta_{0.8-x}Nb_x)_{2/3}Ti_{0.2}]O_2$ and (b) $[(Mg_{0.2}Zn_{0.6})_{1/3}(Ta_{0.8-y}Nb_y)_{2/3}Ti_{0.2}]O_2$. (◇) Trirutile, (△) rutile, (○) tri-αPbO_2, and (□) columbite structures.

lower in the present cases. Then the tri-αPbO_2 finally became the predominant structure at $y = 0.6$. At $y = 0.8$, the columbite structure emerged (similar to the case of $x = 0.8$), leading to the coexistence of tri-αPbO_2 and columbite, along with minor fractions of rutile. It is quite interesting to note that the tri-αPbO_2 structure of $ZnTa_2O_6$ component were detected very widely (even up to the Nb-rich compositions), $0.2 \leq x \leq 0.8$ and $0.0 \leq y \leq 0.8$ in the two systems. Additionally, the tri-αPbO_2 was the major structure developed at $0.2 \leq x \leq 0.6$ and $0.2 \leq y \leq 0.8$.

Phases developed (after the addition of PbO and proper calcinations) in $Pb[(Mg_{0.4}Zn_{0.4})_{1/3}(Ta_{0.8-x}Nb_x)_{2/3}Ti_{0.2}]O_3$ (System I) and $Pb[(Mg_{0.2}Zn_{0.6})_{1/3}(Ta_{0.8-y}Nb_y)_{2/3}Ti_{0.2}]O_3$ (System II) were mostly perovskite, along with parasitic pyrochlore detected at $x = 0.0$–0.4, and $y = 0.4$ and 0.6. In contrast, pyrochlore was the major phase at $y = 0.0$. Minor fractions of ZnO (ICDD No. 36-1451) were also detected, but only in pyrochlore-prone compositions of $y = 0.0$–0.4. The presence of ZnO was believed to have resulted from

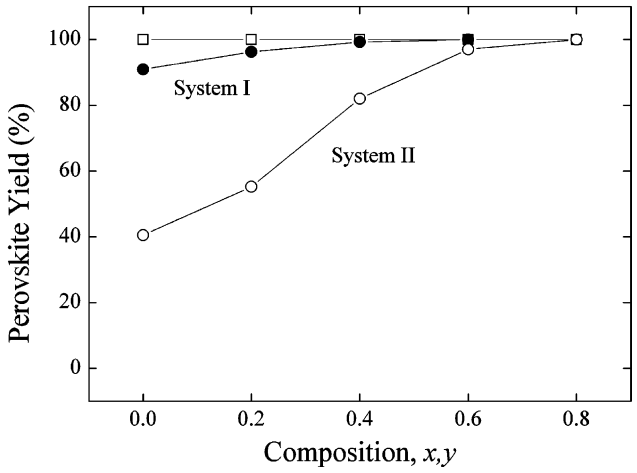

Fig. 2. Perovskite formation yields in $Pb[(Mg_{0.4}Zn_{0.4})_{1/3}(Ta_{0.8-x}Nb_x)_{2/3}Ti_{0.2}]O_3$ (System I) and $Pb[(Mg_{0.2}Zn_{0.6})_{1/3}(Ta_{0.8-y}Nb_y)_{2/3}Ti_{0.2}]O_3$ (System II). Respective values (□) in the system 0.6PMN-0.2PZN-0.2PT with Nb replaced by Ta are also contrasted.

pyrochlore formation from powders of the perovskite stoichiometry. Perovskite contents in Systems I and II were estimated from the X-ray diffractograms of the atmosphere powders (used during the sintering stage) by quantitative comparison as $I_{perov.}/(I_{perov.}+I_{pyro.})$ and the results are plotted in Fig. 2. Values of the 0.6PMN-0.2PZN-0.2PT with Nb replaced by Ta [7] are also included (□) for comparison. Determined values in the two systems were 91% ($x = 0.0$), 96% ($x = 0.2$), and >99% ($0.4 \leq x$), and 40% ($y = 0.0$), 55% ($y = 0.2$), 82% ($y = 0.4$), 97% ($y = 0.6$), and 100% ($y = 0.8$). The values in both systems increased gradually with the Nb fractions of x and y. Moreover, the perovskite yields of System I were somewhat lower than the previous result (□), but were substantially higher than those of System II. The progressive decreases in the perovskite contents are obviously attributable to the increasing fractions of Zn (with lower ionicity in the oxide [12]), which replaces Mg. Relative densities of the sintered ceramics were 93–96% ($x =$ 0.0–0.8), and 87% ($y = 0.0$) and 93–95% ($y = 0.2$–0.8) of theoretical in Systems I and II, respectively.

Representative dielectric constant and loss values of $x = 0.4$ (System I) and $y = 0.4$ (System II) are plotted against temperature and frequency in Fig. 3. Typical frequency-dependent dielectric relaxation with diffuse modes in the phase transition is well demonstrated in both compositions. Values of the maximum dielectric constant and dielectric maximum temperature were 23,400 (77 °C), 22,400 (80 °C), 21,400 (83 °C), and 20,900 (87 °C) for $x = 0.4$ and 7580 (119 °C), 7430 (120 °C), 7310 (123 °C), and 7230 (125 °C) for $y = 0.4$ at 1, 10, 100, and 1000 kHz, respectively. Meanwhile, maximum dielectric losses and corresponding temperatures were 5, 6, 8, and 14% ($x =$ 0.4), and 2.5, 3.5, 4.5, and 7% ($y = 0.4$) in the same frequency decades. Temperatures of the maximum dielectric loss were 15–16 °C (System I) and 30–44 °C (System II) lower than respective dielectric maximum temperatures.

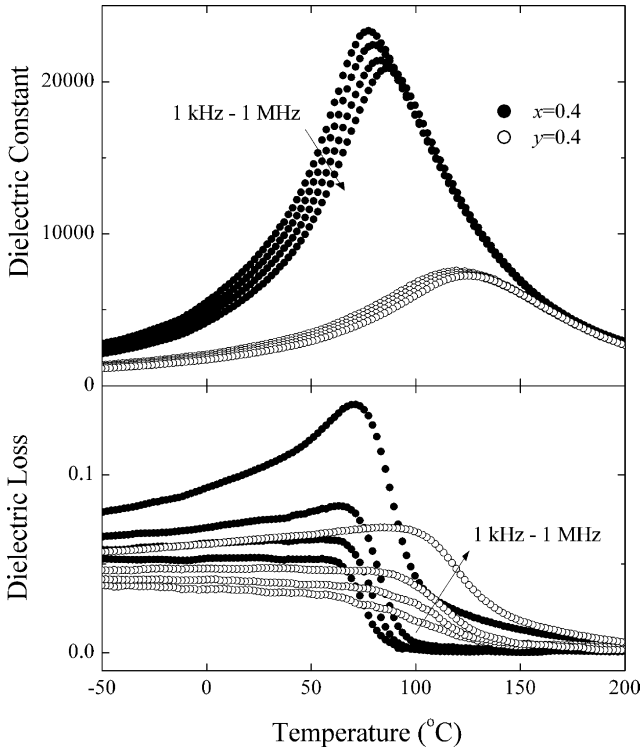

Fig. 3. Typical dielectric relaxation of $x,y = 0.4$ in the frequency range of 1 kHz–1 MHz.

Other compositions of the systems also showed similar dispersion behavior. Dielectric constant spectra of the two system ceramics are contrasted in Fig. 4, in which all of the spectra (including those of $y = 0.0$ and 0.2) were quite diffuse in the phase transition.

Composition- and frequency-dependent values of the maximum dielectric constant and corresponding temperature of the two systems are plotted in Fig. 5. Maximum dielectric constant values (1 kHz) were 13,300 ($x = 0.0$), 19,100 ($x = 0.2$), 23,400 ($x = 0.4$), 28,900 ($x = 0.6$), and

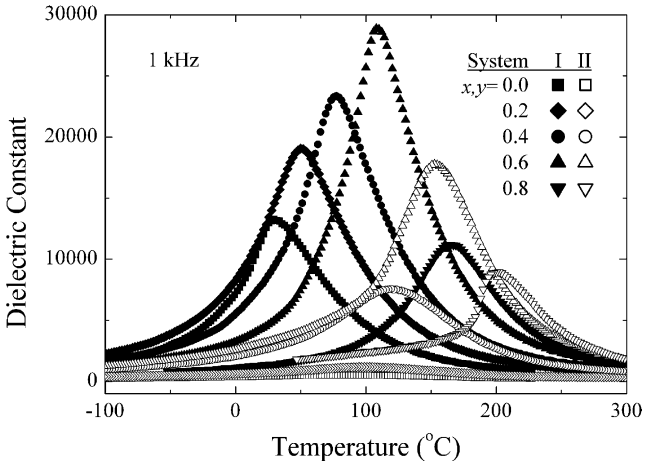

Fig. 4. Temperature-dependent dielectric constant values of the ceramics in the two systems.

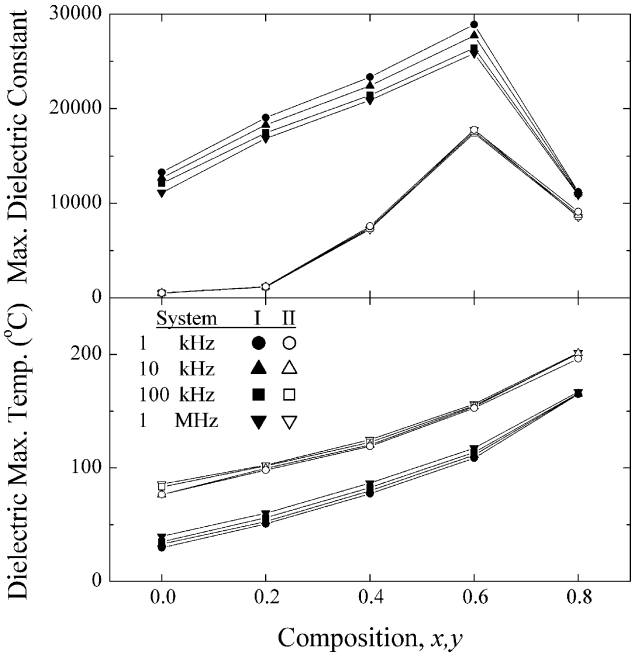

Fig. 5. Variations of the maximum dielectric constant and dielectric maximum temperature with compositional and frequency changes.

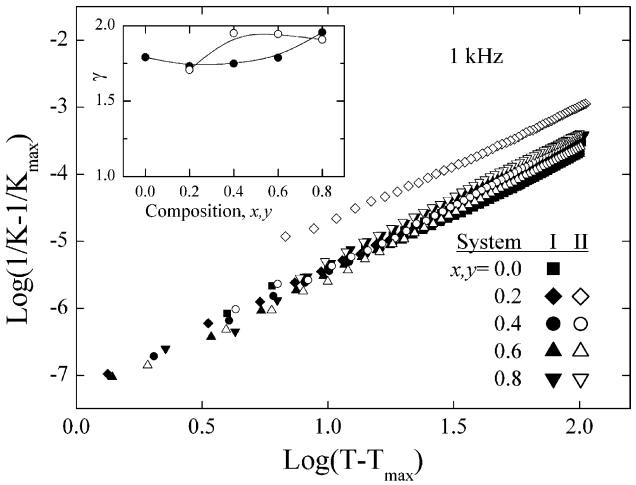

Fig. 6. $\log(1/K - 1/K_{max})$ vs. $\log(T - T_{max})$ of the system ceramics. Estimated values of the diffuseness exponent (γ) are included in the inset.

11,200 ($x = 0.8$) in System I, and 520 ($y = 0.0$), 1190 ($y = 0.2$), 7580 ($y = 0.4$), 17,800 ($y = 0.6$), and 9110 ($y = 0.8$) in System II. Besides, ratios of the maximum dielectric constants ($K_{max,1\,MHz}/K_{max,1\,kHz}$) in System I increased steadily from 84% ($x = 0.0$) to 97% ($x = 0.8$), whereas the values were nearly constant at 94–95% ($y = 0.0$–0.8) in System II. Meanwhile, dielectric maximum temperatures increased in both systems: from 30 °C ($x = 0.0$) to 51 °C ($x = 0.2$), 77 °C ($x = 0.4$), 109 °C ($x = 0.6$), and 165 °C ($x = 0.8$), and from 77 °C ($y = 0.0$) to 98 °C ($y = 0.2$), 119 °C ($y = 0.4$), 153 °C ($y = 0.6$), and 196 °C ($y = 0.8$).

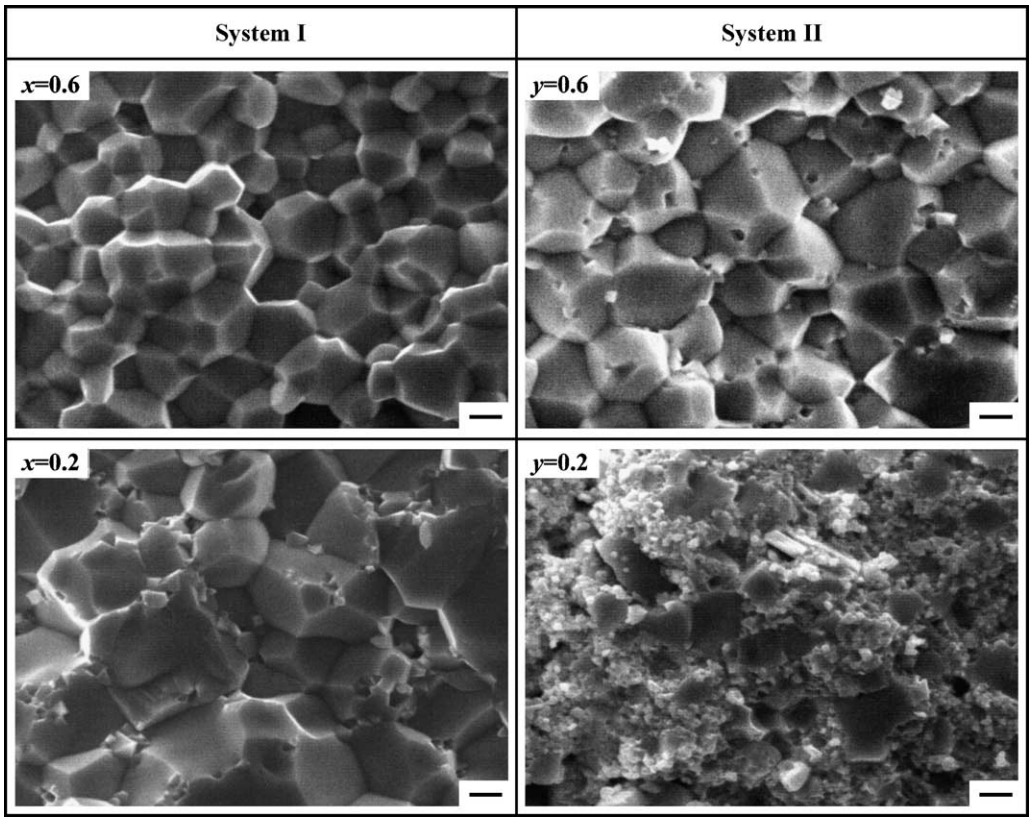

Fig. 7. SEM photomicrographs of the ceramics $x,y = 0.2$ and 0.6. Scale bar = 1 μm.

The maximum dielectric constant values of the present systems were significantly lower with somewhat higher dielectric maximum temperatures, when compared with the results of the Ta-substituted 0.6PMN-0.2PZN-0.2PT system [7]. Such differences are believed to be associated with the role of Zn fractions in the present study.

Dielectric constant spectra above the maximum temperatures are frequently analyzed to quantify diffuseness modes in the phase transition. Relationships of $\log(1/K - 1/K_{max})$ versus $\log(T - T_{max})$ for the two system compositions are shown in Fig. 6. The diffuseness exponent, γ, is a relative measure of the diffuseness. Physical meaning and derivation method of γ can be found elsewhere [13–15]. The γ values were estimated from the slopes of the log-log relations and are separately plotted in the inset of Fig. 6. The values were quite high (1.73–1.96 and 1.71–1.95 in the two systems, respectively), supporting the diffusivity in the phase transition (as observed in the dielectric constant spectra, Fig. 4). Besides, the γ values were rather insensitive to the compositional change.

Fracture-surface micrographs of several compositions are compared in Fig. 7. At $x = 0.2$ (where the perovskite yield was 96%), submicrometer-sized pyrochlore grains were scattered in the perovskite matrices. Meanwhile, only well-developed polyhedral perovskite grains (average size = 2.6 μm) were observed at $x = 0.6$ (perovskite yield = 100%) with few intergranular porosities. In contrast, the fractograph of $y = 0.2$ (perovskite yield = 55%) was composed of scattered perovskite grains in the pyrochlore matrices. The microstructure of $y = 0.6$ (perovskite yield = 97%) was similar to that of $x = 0.2$, but morphologies of the perovskite grains were more rounded with somewhat larger sizes (3.5 μm). In general, fractomicrographs of other compositions were also consistent with the perovskite formation yields.

4. Summary

In the B-site precursor systems of $[(Mg_{0.4}Zn_{0.4})_{1/3}(Ta_{0.8-x}Nb_x)_{2/3}Ti_{0.2}]O_2$ and $[(Mg_{0.2}Zn_{0.6})_{1/3}(Ta_{0.8-y}Nb_y)_{2/3}Ti_{0.2}]O_2$, stability ranges of the tri-αPbO_2 structure of $ZnTa_2O_6$ component were widest (even up to the Nb-rich compositions), $0.2 \le x \le 0.8$ and $0.0 \le y \le 0.8$. Besides, intensities of the tri-αPbO_2 were highest at $0.2 \le x \le 0.6$ and $0.2 \le y \le 0.8$. Moreover, trirutile and columbite were the major structures developed at x, $y = 0.0$ and $x = 0.8$, respectively. After proper reactions of the precursor powders with PbO, perovskite was the major structure developed, along with (parasitic) pyrochlore at Nb-poor compositions. Perovskite formation yields increased steadily with the Nb fraction, with the values of System I considerably higher than those of System II.

Entire compositions of the two systems exhibited dielectric relaxation behavior of frequency dependence, along with diffuse modes in the phase transition. Dielectric constant values of the two systems were maximized to be 28,900 ($x = 0.6$) and 17,800 ($y = 0.6$) at 1 kHz, whereas dielectric maximum temperatures increased linearly in the ranges of 30–165 °C (System I) and 77–196 °C (System II). The diffuseness exponents (γ) were quite high and rather insensitive to the compositional change in the two systems. Microstructures of the fractured ceramics were generally consistent with the perovskite yields.

Acknowledgements

This work was supported by a grant from the Korea Sanhak (Industry-Academy) Foundation (#2001-0145).

References

[1] M. Orita, H. Satoh, K. Aizawa, K. Ametani, Preparation of ferroelectric relaxor $Pb(Zn_{1/3}Nb_{2/3})O_3$–$Pb(Mg_{1/3}Nb_{2/3})O_3$–$PbTiO_3$ by two-step calcination method, Jpn. J. Appl. Phys. 31 (9B) (1992) 3261–3264.
[2] F. Bossler, P. Escure, M. Lejeune, J.P. Mercurio, Dielectric and piezoelectric properties of $PbMg_{1/3}Nb_{2/3}O_3$–$PbTiO_3$–$PbZn_{1/3}Nb_{2/3}O_3$ ceramics, Ferroelectrics 138 (1–4) (1993) 103–112.
[3] P. Escure, E. Lattard, M. Lejeune, J.F. Baumard, Stability of the perovskite phase in PMN–PZN–PT ceramics, J. Mater. Sci. 31 (15) (1996) 3937–3943.
[4] D.-H. Lee, N.-K. Kim, J. Ko, Perovskite phase developments and dielectric properties of PMN-substituted PZN–PT system, Mater. Res. Bull. 34 (14/15) (1999) 2185–2191.
[5] D.-H. Lee, N.-K. Kim, Preparation and dielectric characteristics of perovskite ceramic system 0.8 $Pb[(Mg,Zn)_{1/3}Nb_{2/3}]O_3$–$0.2PbTiO_3$, Ferroelectrics 248 (1–4) (2000) 5–13.
[6] D.-H. Suh, D.-H. Lee, N.-K. Kim, Dielectric properties of the perovskite system $Pb(Mg_{1/3}Nb_{2/3})O_3$–$PbTiO_3$ modified by $Pb(Mg_{1/3}Ta_{2/3})O_3$ and $Pb(Zn_{1/3}Nb_{2/3})O_3$, J. Am. Ceram. Soc. 84 (6) (2001) 1281–1285.
[7] J.-S. Kim, N.-K. Kim, J.-H. Kim, Synthesis and dielectric/ferroelectric characteristics of Ta-modified $PMN_{0.6}$·$PZN_{0.2}$·$PT_{0.2}$ ceramics, J. Mater. Sci. Mater. Electron. 15 (5) (2004) 307–311.
[8] B.-H. Lee, N.-K. Kim, J.-J. Kim, S.-H. Cho, Perovskite formation sequence by B-site precursor method and dielectric properties of PFW-PFN ceramics, Ferroelectrics 211 (1–4) (1998) 233–247.
[9] S.L. Swartz, T.R. Shrout, Fabrication of perovskite lead magnesium niobate, Mater. Res. Bull. 17 (10) (1982) 1245–1250.
[10] S. Ananta, N.W. Thomas, A modified two-stage mixed oxide synthetic route to lead magnesium niobate and lead iron niobate, J. Eur. Ceram. Soc. 19 (2) (1999) 155–163.
[11] M.-C. Chae, N.-K. Kim, J.-J. Kim, S.-H. Cho, Preparation and dielectric properties of $Pb[(Mg_{1/3}Ta_{2/3}), (Zn_{1/3}Nb_{2/3})]O_3$ relaxor ceramics, Ferroelectrics 211 (1–4) (1998) 25–39.
[12] W.F. Smith, Principles of Materials Science and Engineering, 2nd ed., McGraw-Hill, Singapore, 1990, p. 37.
[13] K. Uchino, S. Nomura, Critical exponents of the dielectric constants in diffused-phase-transition crystals, Ferroelectrics Lett. 44 (3) (1982) 55–61.
[14] S.J. Butcher, N.W. Thomas, Ferroelectricity in the system $Pb_{1-x}Ba_x(Mg_{1/3}Nb_{2/3})O_3$, J. Phys. Chem. Solids 52 (4) (1991) 595–601.
[15] M. Kuwabara, S. Takahashi, K. Goda, K. Oshima, K. Watanabe, Continuity in phase transition behavior between normal and diffuse phase transitions in complex perovskite compounds, Jpn. J. Appl. Phys. 31 (9B) (1992) 3241–3244.